Supporting Information

1. Experimental section

1.1. Material

None of the following substances required further purification. Aniline, zinc sulfate ($ZnSO_4$), manganese sulfate ($MnSO_4$), sodium hydroxide, ammonium persulfate ($N_2H_8S_2O_8$), dilute hydrochloric acid, etc. were purchased from Anegis Chemical, carbon cloth was purchased from Guangdong Cloud Company, and zinc foil (100 μm) was purchased from Beijing Saibo.

Synthesis of polyaniline with H ions (PAH) and polyaniline doped with Mn ions (PAM)

0.365 mL of aniline and 1 mL of dilute hydrochloric acid were dissolved in 10 mL of distilled water and configured in a 50 mL beaker. The carbon cloth was placed in the beaker and kept stirring in an ice-water bath for 0.5 h. Then 228 mg of ammonium persulfate was added. After stirring for 1 h, the surface of the carbon cloth was rinsed with ethanol and water, and finally dried to obtain a dark green surface, i.e., PAH. The PAH was soaked in 0.1 mol-L^{-1} NaOH solution for one hour. The PAH was placed in a sealed bottle containing 20 ml of 2 mol L^{-1} $MnSO_4$ solution and prepared at different temperatures and concentrations, i.e., PAM. 48 h at room temperature was labeled as PAM-R and 48 h at 60 °C was labeled as PAM-H. 20 ml of 2,1 and 0.5 mol-L^{-1} $MnSO_4$ solutions were placed in a sealed bottle and labeled as PAM-2, PAM-1 and PAM-2, respectively. PAM-1 and PAM-0.5 were labeled as PAM-2, PAM-1 and PAM-0.5, respectively. After the first step of oxidation and protonation and the second step of deprotonation and Mn doping, the production percentage of PAM is 72.5%.

1.2. Full battery assembly

The full cell was assembled with a 0.1 mm thick zinc foil as the negative electrode, PAM as the positive electrode, glass fiber as the septum (Whatman, GF/C), and 150 μL 2 M $ZnSO_4$ as the electrolyte, i.e., Zn//PAM. The full cell was assembled with 0.1 mm

thick Zn foil as the negative electrode, PAH as the positive electrode, glass fiber as the septum (Whatman, GF/C), and 140 μL 2 M $ZnSO_4$ and 10 μL 2 M $MnSO_4$ as the electrolyte, i.e., Zn//PAH-M. The full cell was assembled with 0.1 mm thick Zn foil as the negative electrode, PAM as the positive electrode, glass fiber as the septum (Whatman, GF/C), and 140 μL 2 M $ZnSO_4$ and 10 μL 2 M $MnSO_4$ as the electrolyte.

Cyclic voltammetry (CV) curves, linear sweep voltammetry (LSV), and electrochemical impedance spectroscopy (EIS) tests from 0.01 Hz to 100 kHz were performed on a CHI 660e electrochemical workstation. Measurement of the multiplicative capacity and cycle stability of the full battery by the constant current charge/discharge (GCD) method on the Xinwei Battery Tester.

Comparison of electrochemical properties (e.g., CV, EIS, LSV, etc.) of PA, PAH, and PAM materials was performed in a three-electrode system with a platinum wire as the reference electrode. Whereas, the full cell performance of the materials (long cycle and multiplicity performance, etc.) was carried out in two electrodes.

1.3. Materials characterization

The crystal structures (PA and PAM) were characterized using X-ray diffraction (XRD, D/max2500pc diffractometer, Cu Kα radiation) in the 2θ range of 10-80°. The morphology of the samples as well as the elemental distribution were obtained by scanning transmission electron microscopy (TEM, JEM-7900) and field emission scanning electron microscopy (SEM, FEI Nova Nano SEM 450) equipped with an energy dispersive spectrometer (EDS). X-ray photoelectron spectroscopy (XPS, Thermo ECALAB 250 with Al anode) with C 1s peak calibration (284.8 eV) was performed to reveal the elemental composition and valence states. Fourier transform infrared spectroscopy (BRUKER VECTOR 22 spectrometer) and laser Raman spectroscopy (InVia-Plus 456 spectrometer) were performed to determine the characteristic groups of the material molecules to analyze the functional group structure.

1.4. Density functional theory calculate

The structures of all systems were optimized based on density functional theory (DFT) at the ωB97XD/def2-SVP level. In the process of optimization, there are no restrictions on the symmetry, bond length, bond angle, or dihedral angle of molecules. Frequency calculations were performed on the optimized structures to ensure that there are no imaginary frequencies, indicating that these structures are stable. All quantum chemical calculations in this work were completed using the Gaussian 16 program package.

Calculate

The energy density (E) and power density (P) of the cathode (or two electrodes) can be calculated according to equations (1) and (2) by the constant current charge/discharge (GCD) test

$$E = \frac{\int QdV}{m} \quad (1)$$

$$P = \frac{E}{t} \quad (2)$$

Q and V represent discharge capacity (Ah or mAh) and voltage (V). m (Kg or g) is the mass of the cathode (or two electrodes), and t (h)is the discharge time.

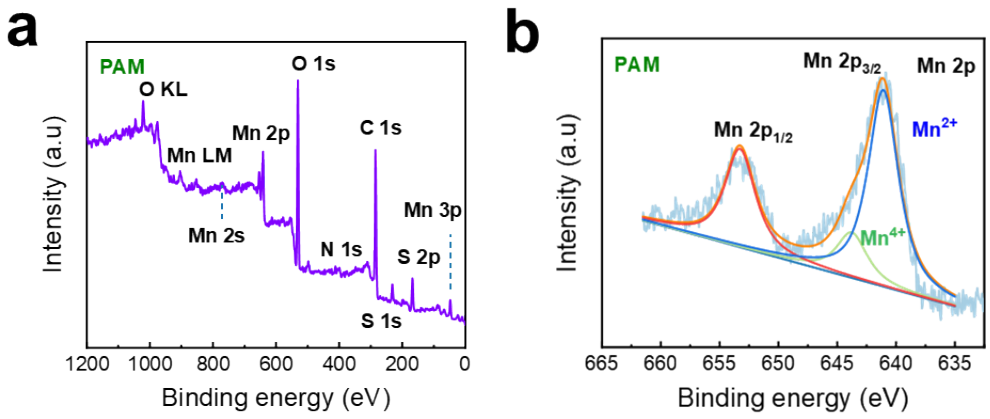

Figure S1. The characteristic diffraction peaks of a) every peak and b) Mn 2p of PAM.

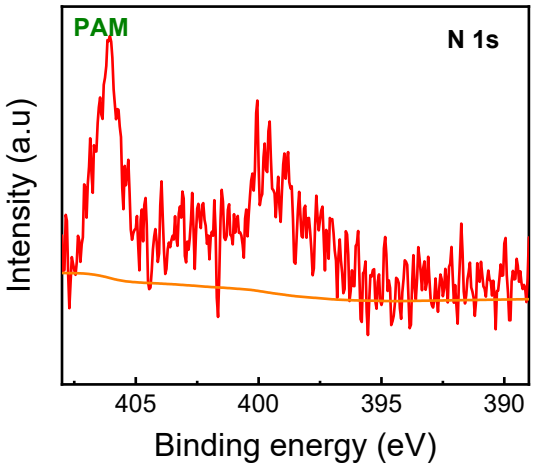

Figure S2. The characteristic diffraction peaks of N 1s of PAM.

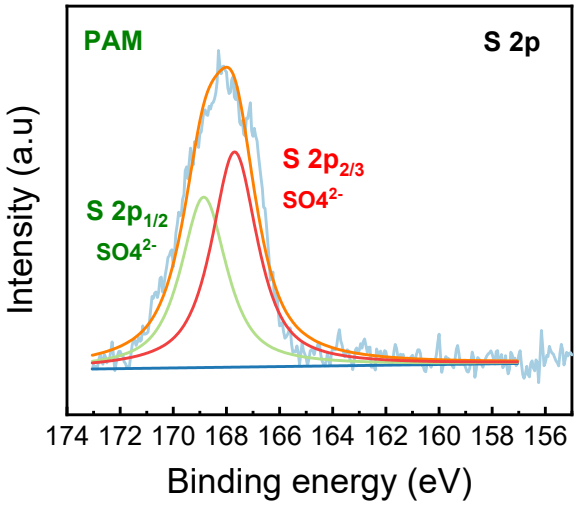

Figure S3. Characteristic diffraction peak pattern of S 2p of PAM.

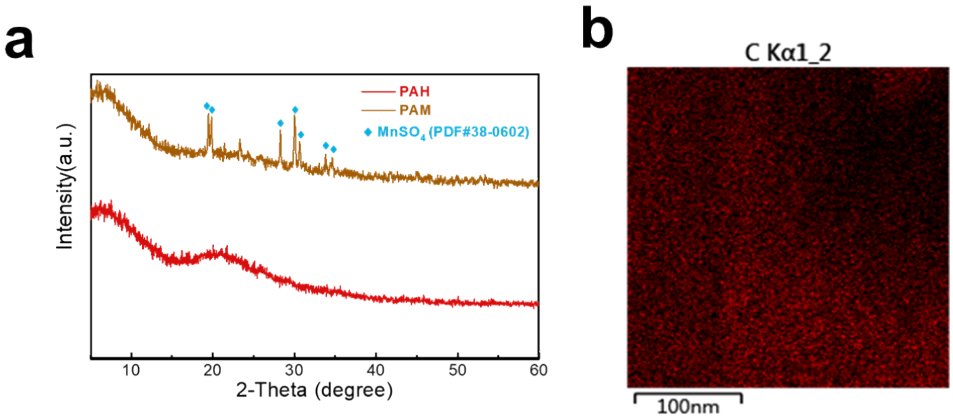

Figure S4. a) XRD pattern of PAM surface after dedoping. b)The C-element distribution of EDX of the PAM active material.

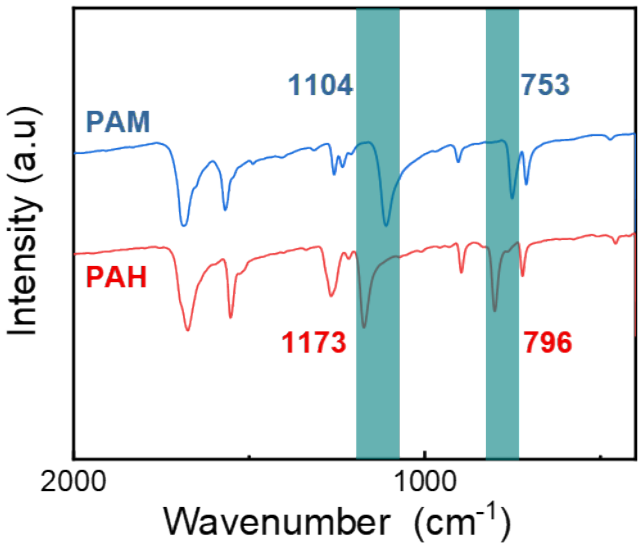

Figure S5. IR tests before (PAH) and after doping (PAM).

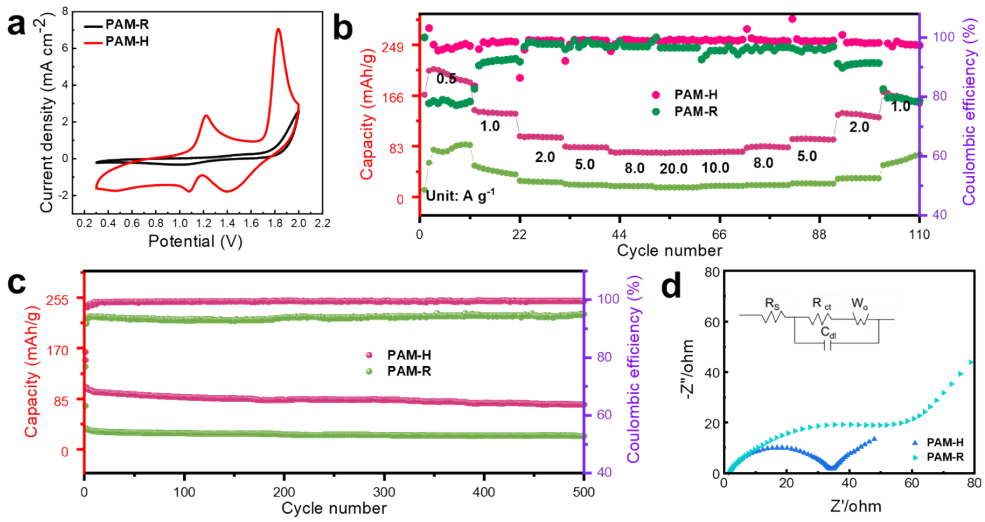

Figure S6. a) CV curves, b) Rate capability, c) GCD long cycle diagram of at current densities of 1 A g^{-1}, and d) EIS curves of PAM-R formed by doping at room temperature and PAM-H material formed by doping under heating.

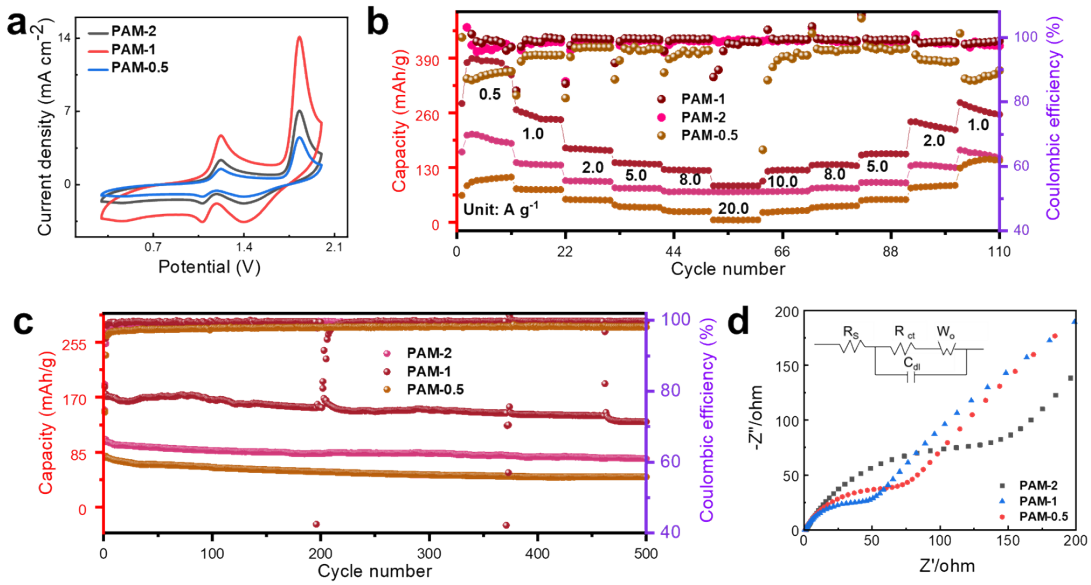

Figure S7. a) CV curves, b) Rate capability, c) GCD long cycle diagram of at current densities of 2 A g^{-1}, and d) EIS curves of different concentrations of doped $MnSO_4$ solutions.

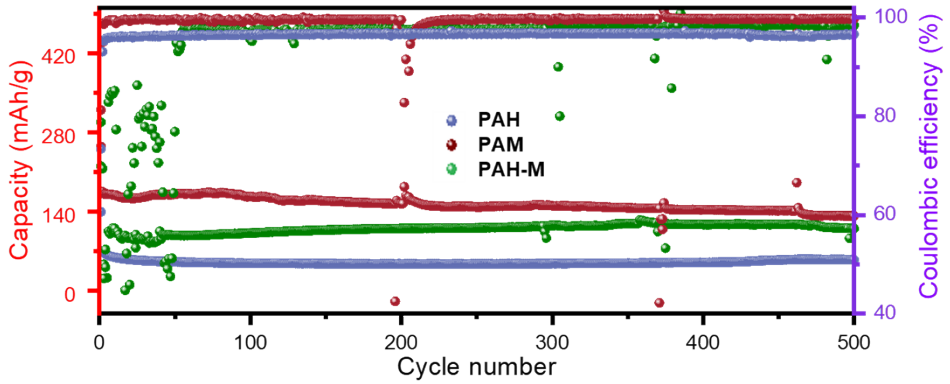

Figure S8. GCD long cycle diagram of at current densities of 3 A g^{-1}.

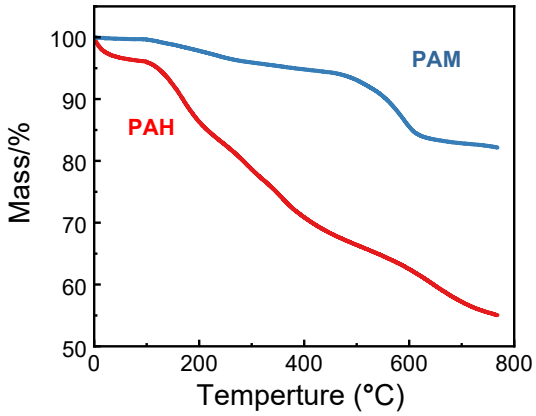

Figure S9. TGA tests before (PAH) and after doping (PAM).

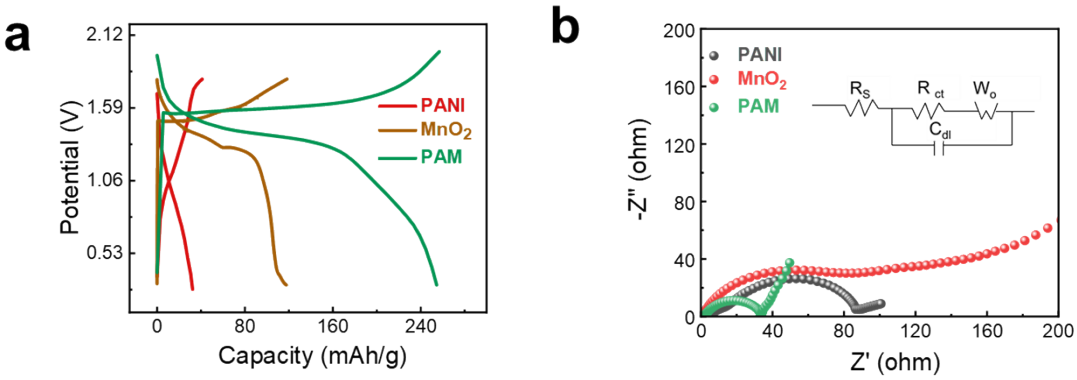

Figure S10. a) Capacity vs. voltage at current densities at 1 A g^{-1} of the cells composed of PANI, MnO_2, and PAM electrodes. And b) EIS curves of PANI, MnO_2, and PAM.

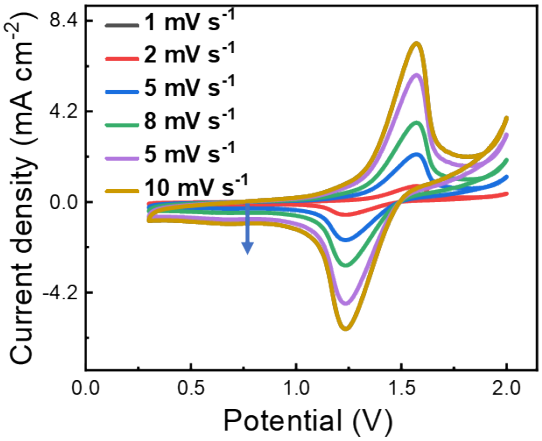

Figure S11. CV curve of Zn//PAH cells at different scan rates of 0.8-10 mV s^{-1}.

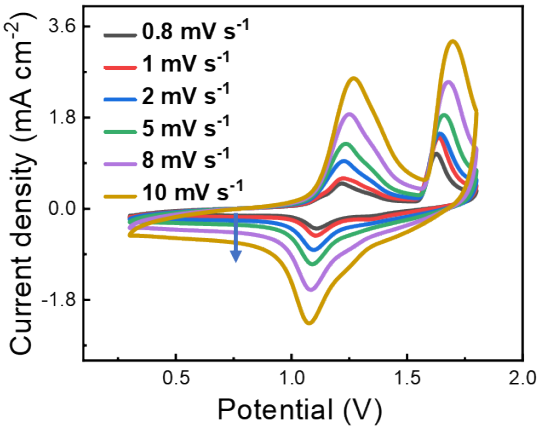

Figure S12. CV curve of Zn//PAM cells at different scan rates of 0.8-10 mV s^{-1}.

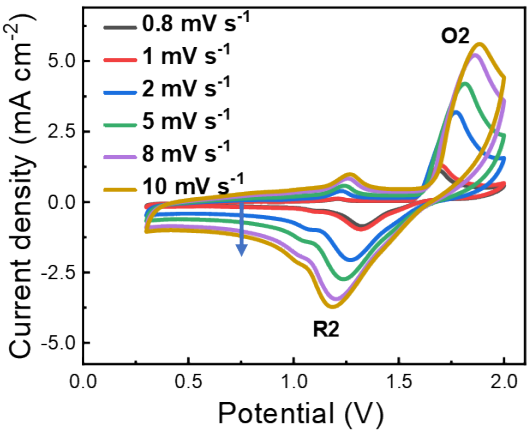

Figure S13. CV curve of Zn//PAH-M cells at different scan rates of 0.8-10 mV s^{-1}.

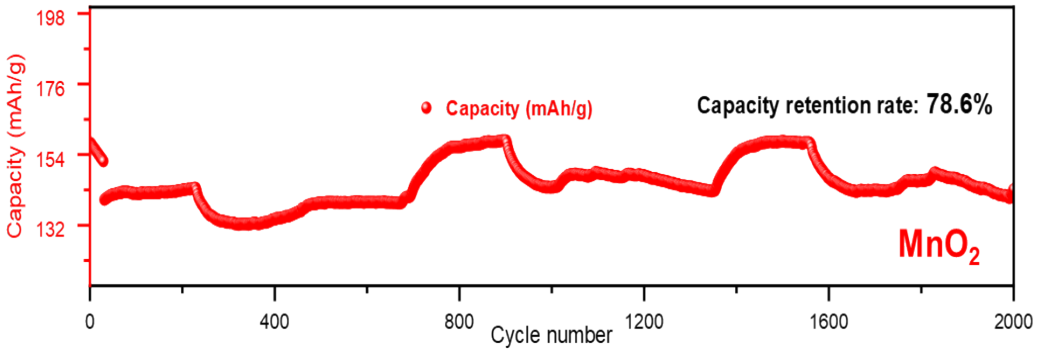

Figure S14. a) Long cycles at current densities at 1 A g^{-1} of the cell with MnO_2.

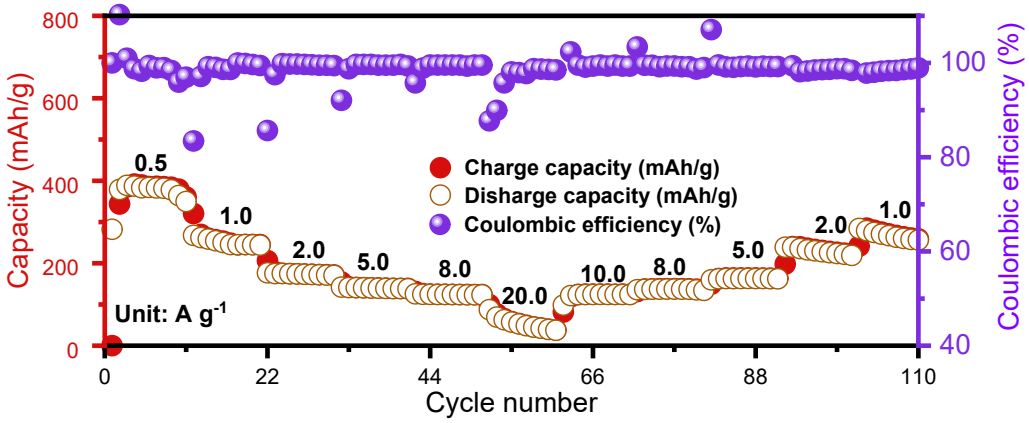

Figure S15. Rate capability of Zn//PAM cell.

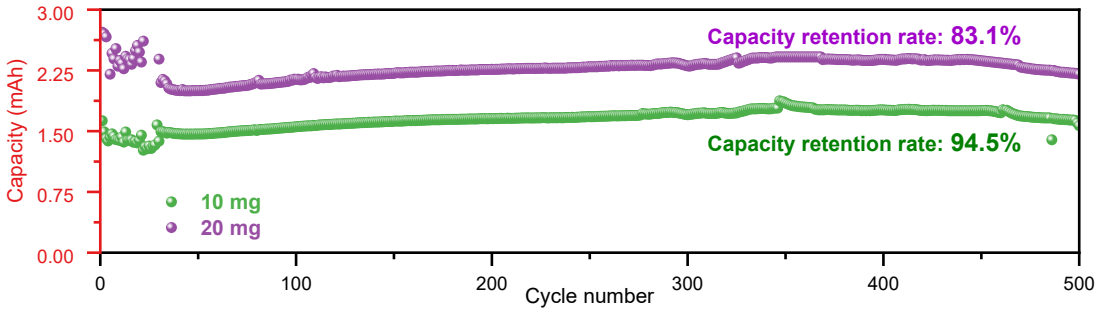

Figure S16. The capacity retention for 500 cycles at a current density of 1 A g^{-1}.

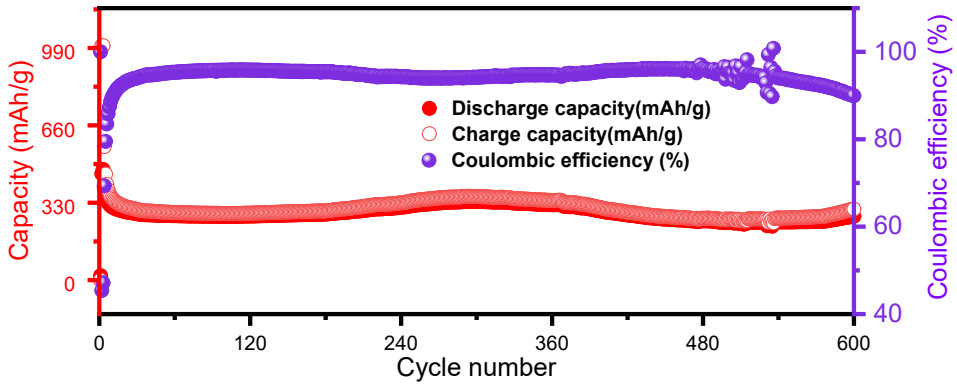

Figure S17. GCD long cycle diagram of Zn//PAM cell in 2.4 V at current densities of 2 A g^{-1}.

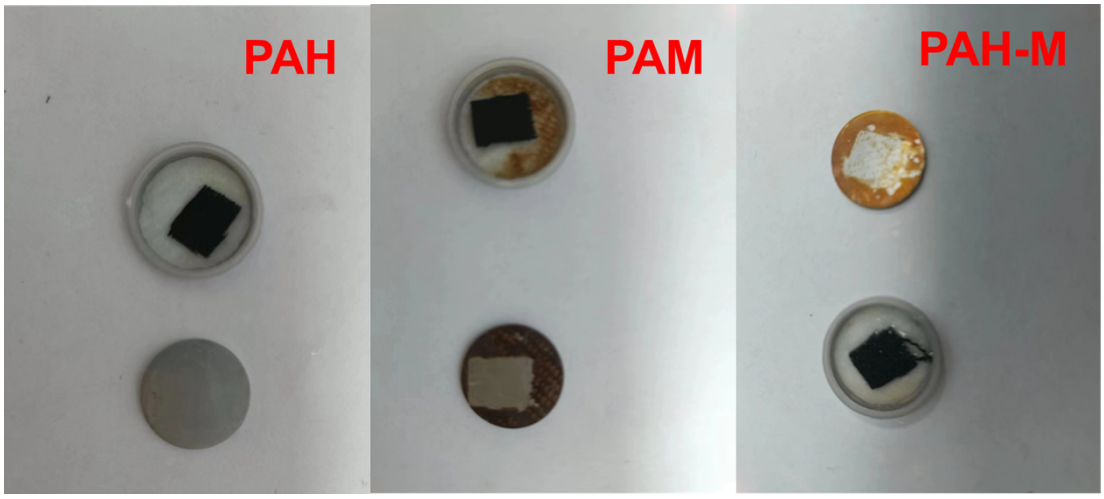

Figure S18. Internal presentation of PAH, PAM, and PAH-M battery disassembly after cycling.

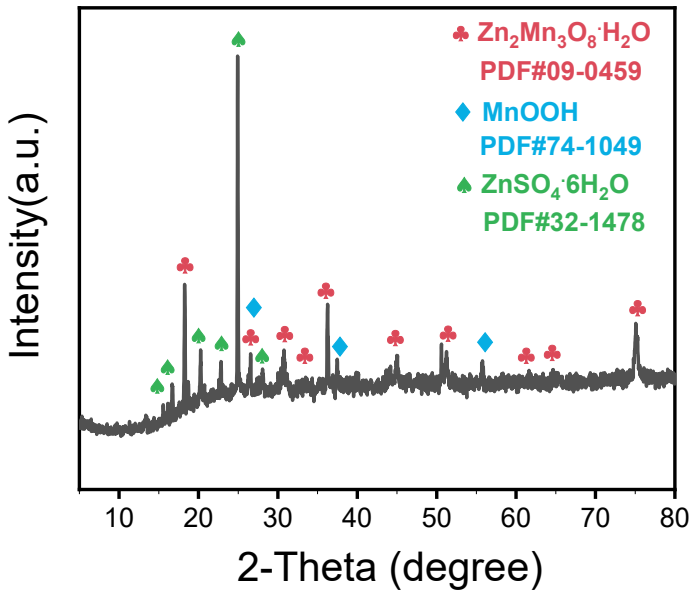

Figure S19. The GCD curve of the site is tested at each stage of the surface of PAM during the cycle. at current densities of 2 A g^{-1}.

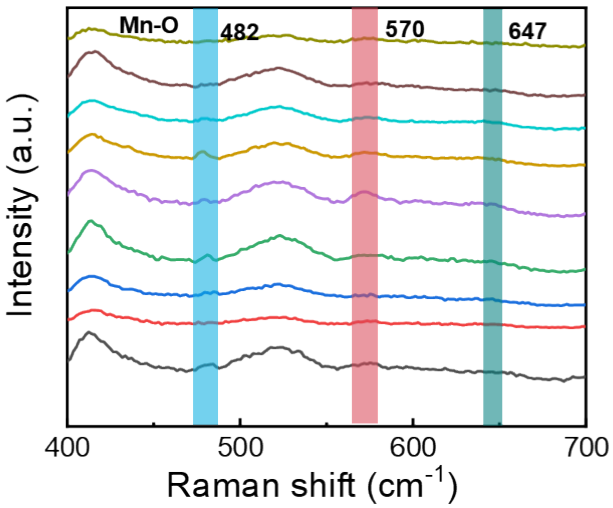

Figure S20. Raman diagram of the PAM surface at 400-700 shifts during cycling.

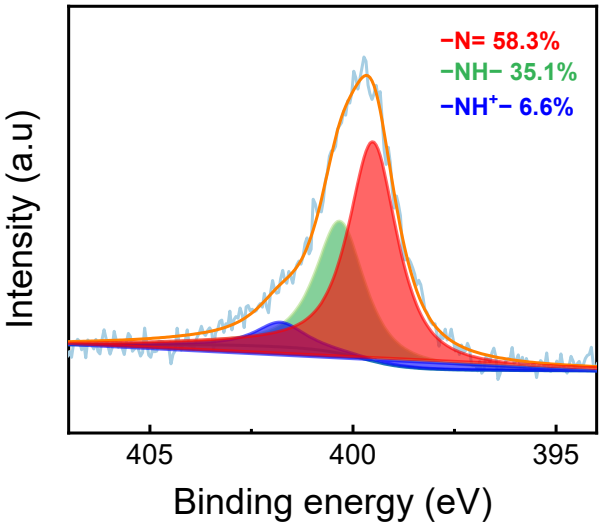

Figure S21. *Ex-situ* N 1s XPS curves at the charging and discharging points between PAM-c and PAM-d.

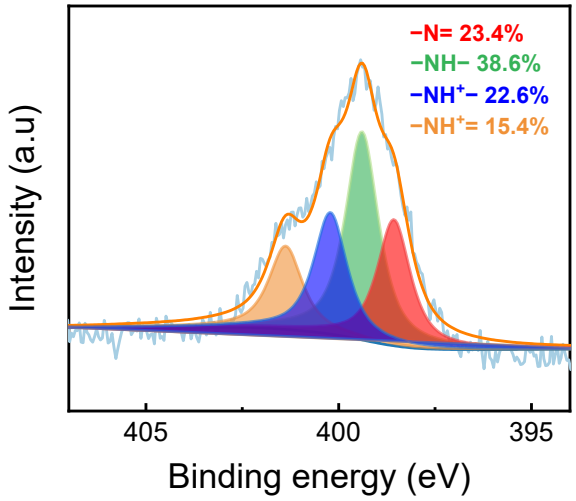

Figure S22. *Ex-situ* N 1s XPS curves at the charging and discharging points between between PAM-e and PAM-f.

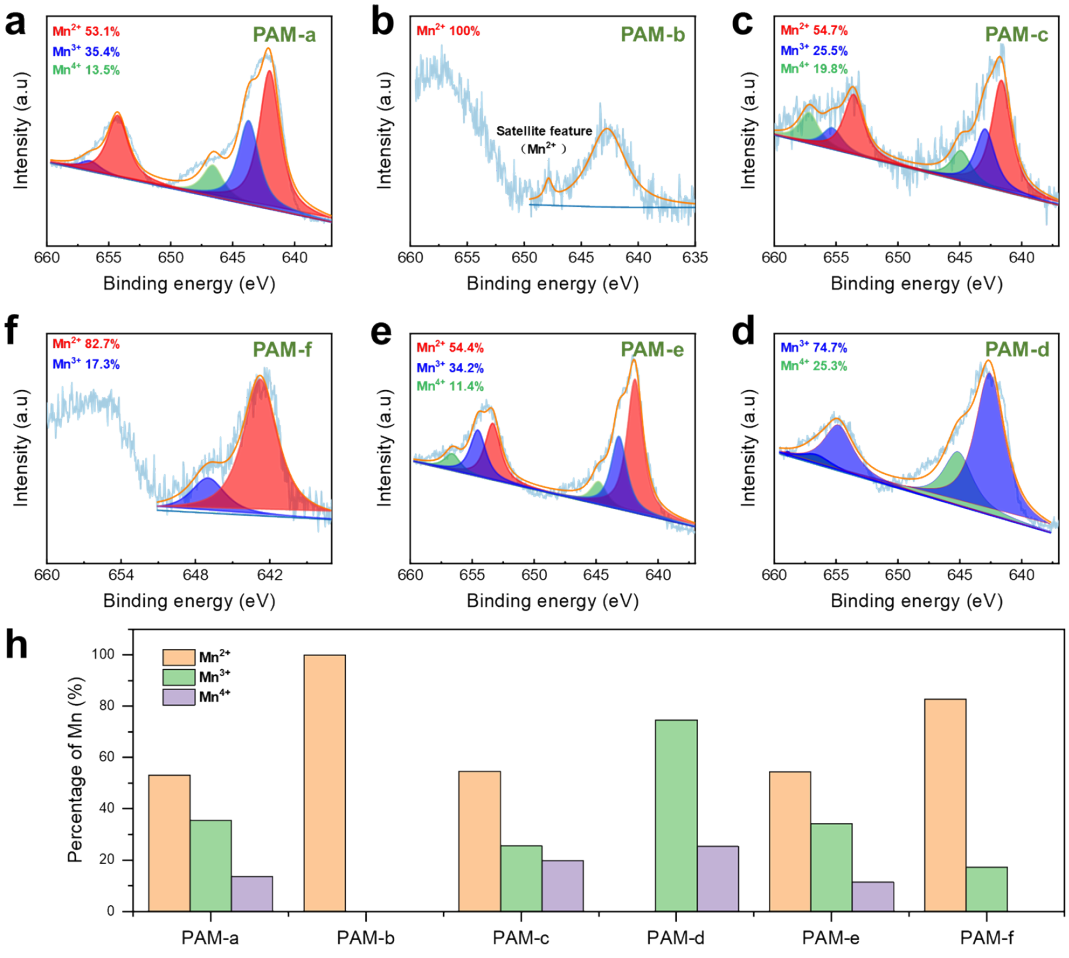

Figure S23. a-b) Ex-situ Mn 2p XPS curves of PAM material during the first turn of

discharge, c-d) Ex-situ Mn 2p XPS curves of PAM material at the second charge, e-f) Ex-situ Mn 2p XPS curves of PAM material at the second discharge, and h) Valence changes of Mn at each stage of the PAM material during cycle.

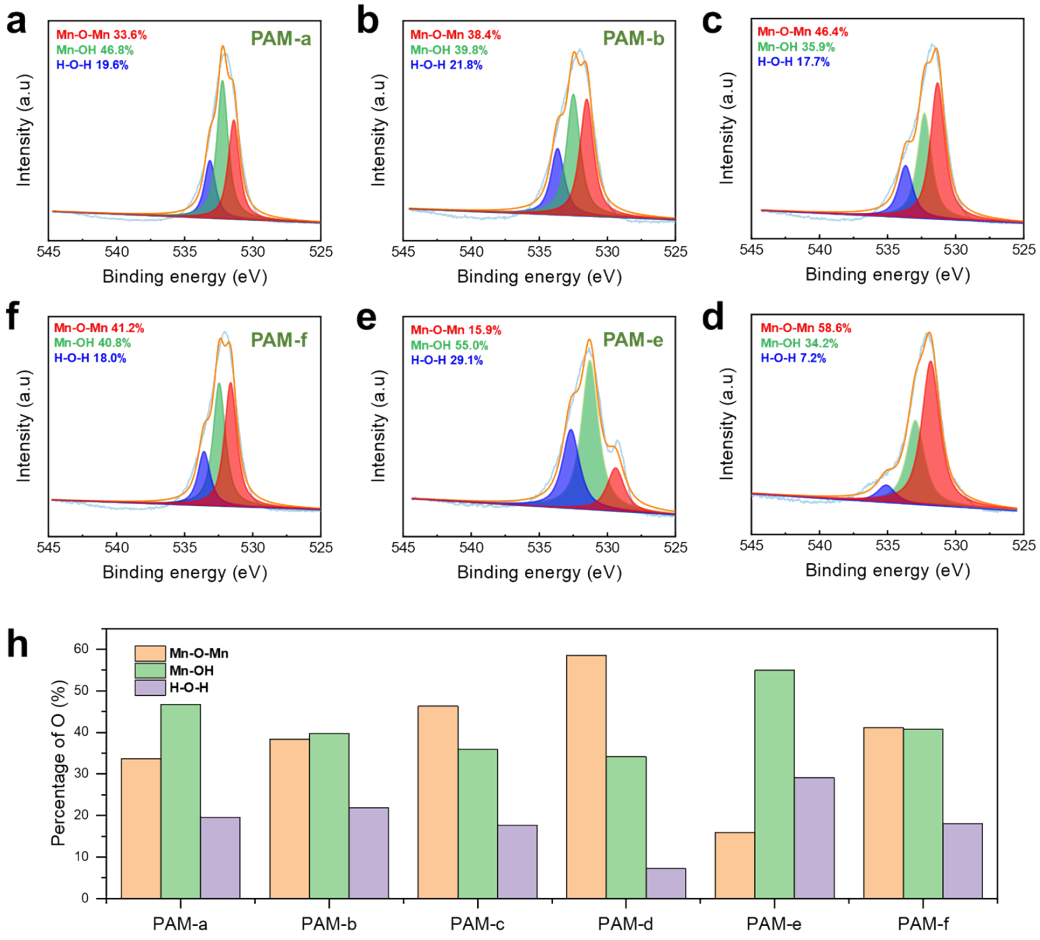

Figure S24. a-b) Ex-situ O 1s XPS curves of PAM material during the first turn of discharge, c-d) Ex-situ O 1s XPS curves of PAM material at the second charge, e-f) Ex-situ O 1s XPS curves of PAM material at the second discharge, and h) Changes in the bonding components of O at each stage of the PAM material during cycle.

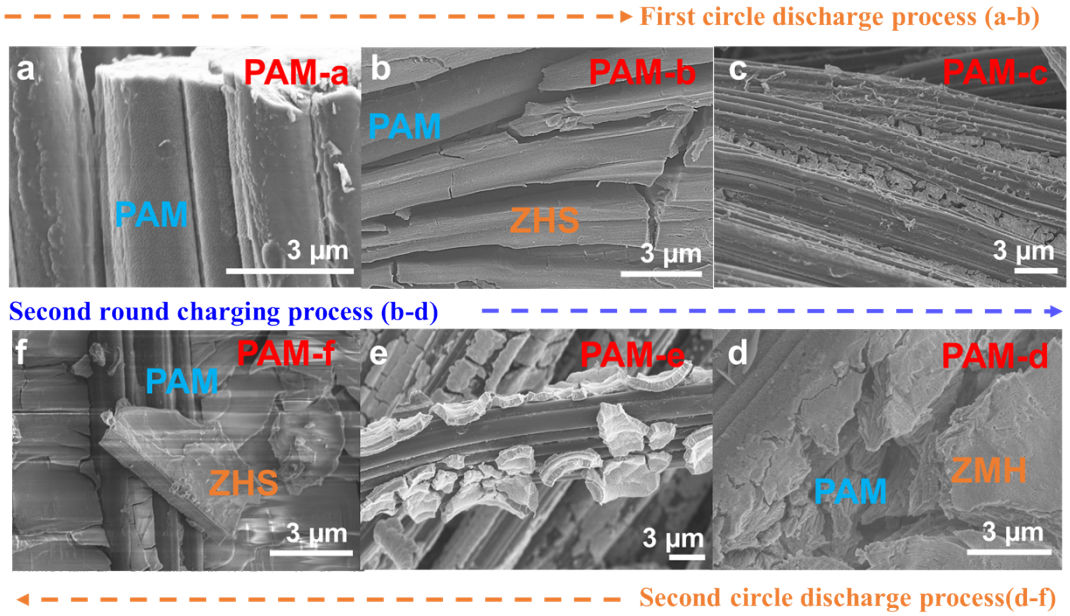

Figure S25. SEM images of PAM electrodes at each stage of the cycle process.

Table S1. Characteristic Raman peaks of PANI and PANI-Mn

Samples	C-H	$C\text{-}N^+$	C=N	C=C
PANI	1163 cm^{-1}	1348 cm^{-1}	1481 cm^{-1}	1592 cm^{-1}
PANI-Mn	1182 cm^{-1}	1354 cm^{-1}	1495 cm^{-1}	1599 cm^{-1}

Table S2. The performance comparison of the Zn//PAM battery and the previously reported aqueous Zn//PANI battery

Aqueous battery	Electrolyte	Maximum specific capacity (mAh g^{-1})	Maximum energy density (Wh kg^{-1})	Reference
Zn//PAM	**$ZnSO_4$**	**388.8**	**330.5**	**This Work**
Zn//PAH		**112.6**	**90.1**	
Zn//PAH-M		**290.8 at 1 A g^{-1}**	**245.3**	
Zn//Au-CNT/PANI	AF-SH-CPAM	233.9 at 0.1 A g^{-1}	244.2	1
Zn// PANI	PVA/$Zn(CF_3SO_3)_2$ hydrogel	123 at 0.1 A g^{-1}	~120	2
Zn// PANI-S	$ZnSO_4$ aqueous solution	184 at 0.2 A g^{-1}	~55	3
Zn//PANI	$Zn(CF_3SO_3)_2$ aqueous solution	200 at 0.05 A g^{-1}	-	4
Zn//PANI/SWCNTs	PNIPAM/AM copolymerized hydrogel	168.7 at 0.1 A g^{-1}	-	5
Zn//Nanostructured Polyaniline-Cellulose	$ZnCl_2$ and NH_4Cl aqueous solution	142.3 at 0.2 A g^{-1}	117.5	6
Zn/SWCNTs-RGO//PANI/SWCNTs	PVA/$Zn(CF_3SO_3)_2$ hydrogel	167.6 at 0.1 A g^{-1}	-	7
Zn//Nickel foam-supported PANI	$ZnSO_4$ aqueous solution	183.28 at 2.5 mA cm^{-2}	-	8
Zn//Polyaniline	PVA/$ZnCl_2$ and NH_4Cl gel electrolyte	~165 at 0.2 A g^{-1}	115	9
Zn//3D graphene@PANI composite	$ZnSO_4$ aqueous solution	175.5 at 0.1 A g^{-1}	-	10
Zn//Graphene@PANI	2 M $ZnSO_4$ aqueous solution	154 at 0.1 A g^{-1}	205	11
Zn//PANI fiber battery	PVA/$ZnCl_2$ and NH_4Cl gel electrolyte	119.41 at 0.1 g^{-1}	-	12
Zn//PANI-V_2O_5	$ZnSO_4$ water/EG solution	180 at 0.1 g^{-1}	121	13
Zn//PANI	$ZnCl_2$ aqueous solution	151.1 at 1 A g^{-1}	-	14
Zn//PANI	$ZnSO_4$ aqueous solution	203.5 at 0.5 A g^{-1}	233.4	15

Zn//PANI-SWCNT-sponge	PVA/Zn(CF_3SO_3)$_2$ hydrogel	212 at 0.1 A g^{-1}	-	16

References

[1] X. Jin, L. Song, C. Dai, H. Ma, Y. Xiao, X. Zhang, Y. Han, X. Li, J. Zhang, Y. Zhao, Z. Zhang, L. Duan, L. Qu, *Energy Storage Mater.* **2022**, 44, 517.

[2] S. Huang, F. Wan, S. Bi, J. Zhu, Z. Niu, J. Chen, *Angew. Chem.* **2019**, 131, 4357.

[3] H. Y. Shi, Y. J. Ye, K. Liu, Y. Song, X. Sun, *Angew. Chem.* **2018**, 130, 16597.

[4] F. Wan, L. Zhang, X. Wang, S. Bi, Z. Niu, J. Chen, *Adv. Funct. Mater.* **2018**, 28, 1804975.

[5] J. Zhu, M. Yao, S. Huang, J. Tian, Z. Niu, *Angew. Chem. Int. Ed.* **2020**, 59, 16480.

[6] Y. Ma, X. Xie, R. Lv, B. Na, J. Ouyang, H. Liu, *ACS Sustain. Chem. Eng.* **2018**, 6, 8697.

[7] M. Yao, Z. Yuan, S. Li, T. He, R. Wang, M. Yuan, Z. Niu, *Adv. Mater.* **2021**, 33, 2008140.

[8] Y. Xia, D. Zhu, S. Si, D. Li, S. Wu, *J. Power Sources* **2015**, 283, 125.

[9] G. Shim, M. X. Tran, G. Liu, D. Byun, J. K. Lee, *Energy Storage Mater.* **2021**, 35, 739.

[10] Y. Zhang, Q. Wang, S. Bi, M. Yao, F. Wan, Z. Niu, *Nanoscale* **2019**, 11, 17630.

[11] J. Han, K. Wang, W. Liu, C. Li, X. Sun, X. Zhang, Y. An, S. Yi, Y. Ma, *Nanoscale* **2018**, 10, 13083.

[12] H. Yu, G. Liu, M. Wang, R. Ren, G. Shim, J. Y. Kim, M. X. Tran, D. Byun, J. K. Lee, *ACS Appl. Mater. Interfaces* **2020**, 12, 5820.

[13] N. Chang, T. Li, R. Li, S. Wang, Y. Yin, H. Zhang, X. Li, *Energy Environ. Sci.* **2020**, 13, 3527.

[14] Q. Zhang, Y. Ma, Y. Lu, L. Li, F. Wan, K. Zhang, J. Chen, *Nat. Commun.* **2020**, 11, 4463.

[15] P. Liu, R. Lv, Y. He, B. Na, B. Wang, H. Liu, *J. Power Sources* **2019**, 410-411, 137.

[16] H. Cao, F. Wan, L. Zhang, X. Dai, S. Huang, L. Liu, Z. Niu, *J. Mater. Chem. A* **2019**, 7, 11734.